Electroreduction of p-Nitrophenol at supported Mono- and Bimetallic Dendrimer Encapsulated Catalysts

Jay S. Croley* and Keith J. Stevenson [a,b,]

Department of Chemistry and Biochemistry, Center for Nano- and Molecular Science and Technology [a], Texas Materials Institute [b],
The University of Texas at Austin, Austin, Texas, 78712

Generation 6 hydroxyl-terminated (G6-OH) polyamidoamine (PAMAM) dendrimers were used as templates to synthesize Au, Cu, Pd, Pt, AuCu, PdCu, and PtCu nanoparticles (DENs). The dendrimer templates act as nanoreactors to control the size of nanoparticles in the range of 1 to 3 nanometers. The DENs were immobilized on glassy carbon electrodes and investigated as catalysts towards the electrochemical reduction of *para*-nitrophenol (PNP) to *para*-aminophenol (PAP). Particle size distributions of monometallic and bimetallic catalysts were characterized by a combination of transmission electron microscopy, energy dispersive spectroscopy, and UV-Vis spectroscopy. The heterogeneous catalytic activities of the mono- and bimetallic catalysts were assessed using cyclic voltammetry and compared with the homogeneous catalytic activities found using UV-Vis spectroscopy

* To whom correspondence should be addressed.
E-mail: sawyer.croley@gmail.com

Introduction

Nanoparticles are of particular interest in the field of catalysis because of their unique properties when compared to bulk materials. Noble metals such as gold are inert in bulk, but have proven to exhibit high catalytic activities when synthesized on the nanoscale.[1,2] Sanchez et al.[3] have demonstrated the size-selective catalytic activity of gold clusters deposited on magnesium oxide films for CO oxidation. Gold particles as small as eight atoms showed catalytic activity, whereas bulk gold is known to be inactive for CO oxidation. This high chemical reactivity is a result of the increased surface area to volume ratio, which lowers the redox potential value of the particle[2] and creates novel adsorption sites for reactants.[4]

The tendency for metal ions to aggregate into monodisperse nanocrystalline structures requires synthetic templates such as dendrimers.[5] Dendrimers have been the focus of recent catalysis studies because of their ability to control nanoparticle size without substantial blocking of the active catalytic sites.[6] The ability to tune nanoparticles to a narrow size range is essential for (i) investigating the unique catalytic properties that arise as a result of their 1-3 nm size and (ii) making a fair comparison of the relative catalytic activity between the metal species. The choice of the particular dendrimer generation allows for synthesis of nanoparticles in the 1-3 nm size range that have been shown to exhibit unique catalytic properties.[7]

As reported by Zhao et al.[8], G4-NH_2 PAMAM dendrimers can be used to encapsulate and stabilize transition metal atoms such as Cu^{2+} within the dendrimer interior. Initially, the peripheral primary amines are selectively protonated at pH ~3-5. The ability to selectively protonate the exterior is a consequence of the exterior primary amines being more basic (pK_a = 9.23) than the interior tertiary amines (pK_a = 6.30).[9] The metal ions diffuse within the dendrimer and interact with the interior tertiary amines. At pH 3, a maximum of 65 ± 5 Cu^{2+} ions can be concentrated inside each PAMAM G4-NH_2 dendrimer.[9] The number of metal atoms per cluster corresponds with the number of available tertiary amines within the dendrimer.[8] However above pH 5, metal ions are not extracted from solution because of their affinity for the peripheral functional groups. This causes the ions bind to the exterior of the dendrimer which leads to agglomeration. With the addition of a reducing agent, the metal ions are reduced to the zero valent state forming nanoparticles 1 to 3 nanometers in diameter. Generation 6 hydroxyl terminated dendrimers (G6-OH) DENs can also be used without the need for pH adjustments to

template nanoparticles as large as 240 atoms. The interior amine functionalities complex the metal ions and then are reduced in a similar fashion using $NaBH_4$ (Figure 1).

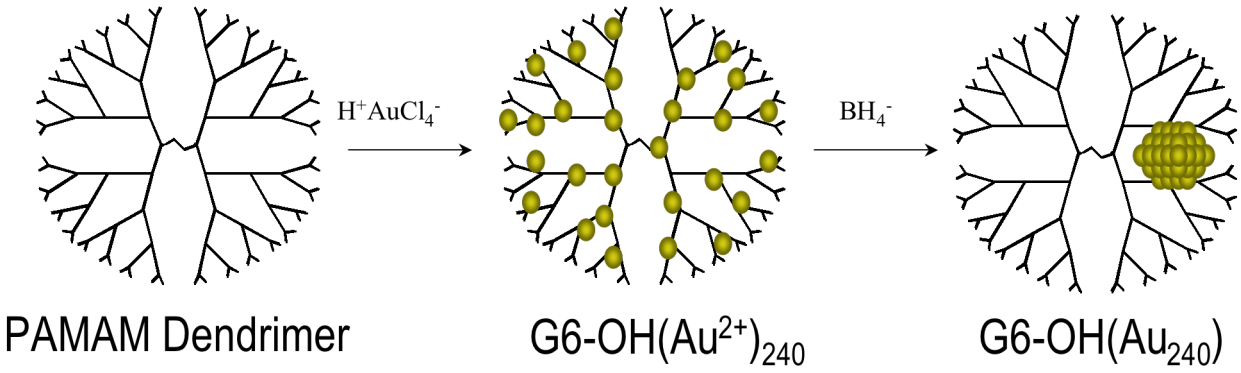

Figure 1: General scheme for synthesis of Au dendrimer encapsulated nanoparticles (Au-DENs)

Here we focus on comparing the homogeneous and heterogeneous catalytic activities of various mono- and bimetallic nanoparticles encapsulated within dendrimer templates. Bimetallic nanoparticles often exhibit synergistic catalytic properties that are significantly better than either of their monometallic components. Endo et al.[10] have demonstrated that 3:1 Au:Ag nanoparticles are more catalytically active than monometallic silver or gold for the reduction of *p*-nitrophenol. In this study we investigated the possibility of enhanced catalysis at AuCu, PtCu, and PdCu alloy systems. While comparisons using a few monometallic transition metals have been reported, an extensive study using Au, Pd, Pt, and Cu has not. Homogeneous catalytic activity was assessed by a model chemical reaction in which *para*-nitrophenol (PNP) was reduced to *para*-aminophenol (PAP) with the addition of BH_4^- (Figure 2). This chemical reaction is known to proceed by either a direct reduction of PNP to PAP, or by a condensation route involving two intermediates.[11]

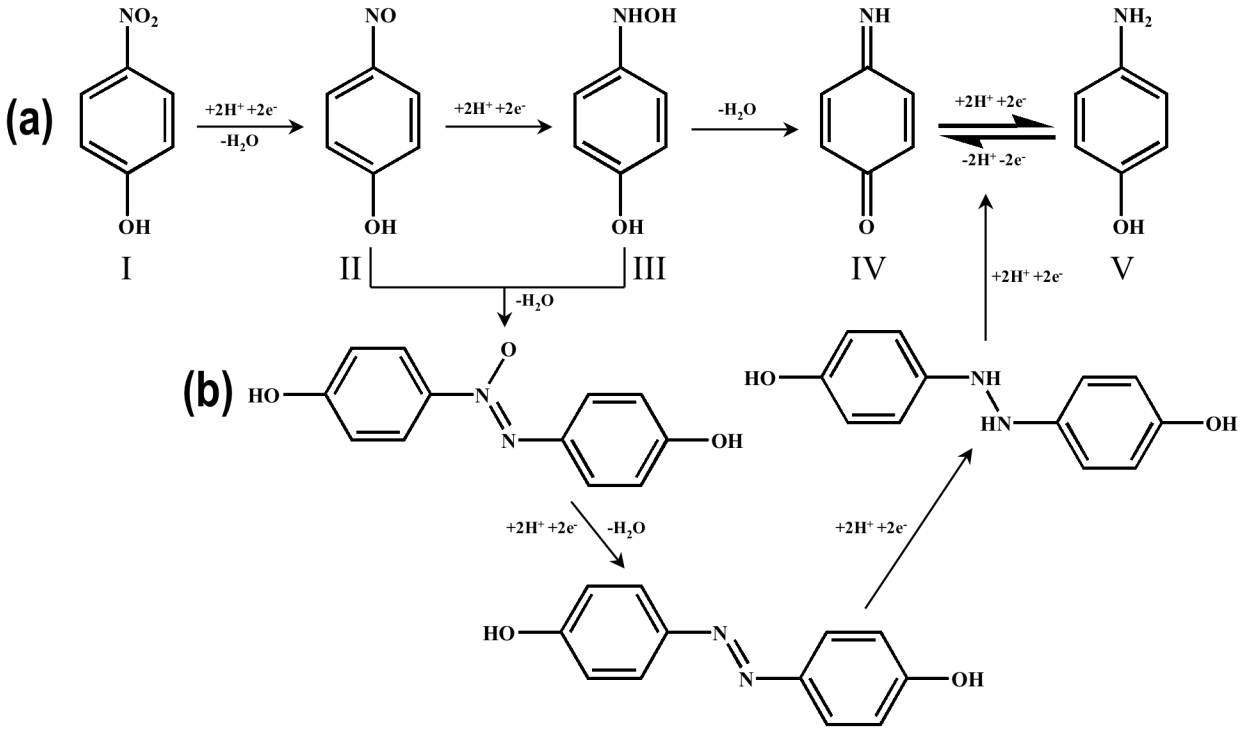

Figure 2. Proposed mechanisms for the reduction of para-nitrophenol to para-aminophenol (a) Direct route (b) Condensation route. I. p-nitrophenol, II. p-nitrosophenol, III. p-hydroxylaminophenol, IV. p-quinoneimine, V. p-aminophenol

Rate constants for each of the nanoparticle catalysts were found by monitoring the absorbance of *p*-nitrophenol using UV-Vis spectroscopy. The characterization protocol is unambiguous because *p*-nitrophenol is not reduced to *p*-aminophenol in the absence of a catalyst and the two species absorb electromagnetic radiation at 400 and 310 nm respectively. Heterogeneous rate constants were determined by supporting the dendrimer encapsulated nanoparticles on glassy carbon electrodes (GCE) and using cyclic voltammetry to reduce PNP to PAP (Figure 3).

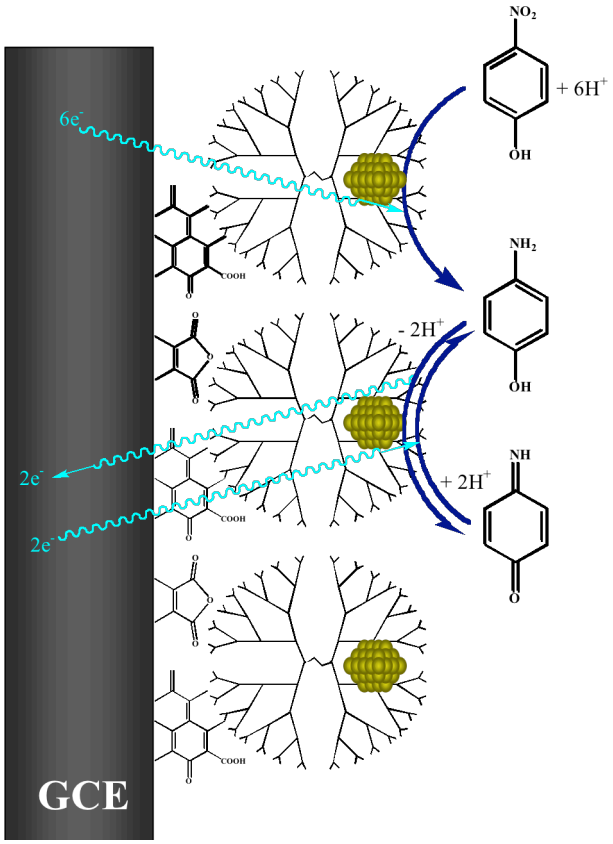

Figure 3 Schematic of G6-OH DENs attached to glassy carbon for the electroreduction of p-nitrophenol to p-aminophenol

Experimental Section

Materials. G6-OH and G4-NH_2 PAMAM dendrimers with an ethylenediamine core were purchased as 10 wt. % solutions in methanol from Dendritech, Inc, Midland, MI. The methanol was evaporated under vacuum at room temperature before use. Reagent grade $HAuCl_4$ (Aldrich), K_2PdCl_4 (Aldrich), K_2PtCl_4 (Aldrich), and $CuSO_4$ (EM Science) were used as precursors. *p*-nitrophenol (Sigma) and $NaBH_4$ (Fischer Scientific) were of analytical grade and used as received. All aqueous solutions were prepared with 18.3 MΩ·cm water. Impurities were removed from DEN solutions by use of 0.20 μm syringe filters (Whatman).

G6-OH dendrimer-encapsulated particles were synthesized by adding 480 μL of a 0.1M metal salt solution to 18.66 mL of a 0.01 mM dendrimer solution. This concentration of metal salt is 240 times molar excess compared with the dendrimer concentration, theoretically yielding 240 atom nanoparticles housed within dendrimer templates. After a pre-determined coordination

period, the drop-wise addition of 960 μL of 0.5M $NaBH_4$ (20 times molar excess) reduced the particles to a zero-valent state. Bimetallic nanoparticles were synthesized by a co-complexation method in which 240 μL of each 0.1M metal salt solution was simultaneously added and allowed to coordinate before the addition of a reducing agent.

In a typical synthesis of G4-NH_2 dendrimer-encapsulated nanoparticles, 50 mL of a 0.01 mM dendrimer solution was prepared at pH 3. 150 μL of 0.1 M metal salt solution (30 times molar excess) was added to the aqueous dendrimer solution. Bimetallic nanoparticles were synthesized by simultaneous addition of the metal salts in 15 times molar excess with respect to the dendrimer. After a pre-determined coordination period, 600 μL of aqueous 0.5 M $NaBH_4$ (20 times molar excess) was added drop-wise and the solution was left stirring for 30 minutes. The addition of sodium borohydride caused a significant increase in pH which was then adjusted to pH 8 using 0.1 M HCl.

Characterization. An Agilent 8453 diode array spectrophotometer was used for all UV-Vis spectroscopy. High resolution transmission electron microscopy images were taken with a JEOL-2010F TEM operating at 200 kV. Samples were drop cast onto a Cu TEM grid covered with a lacey carbon film and allowed to evaporate in air prior to analysis. Average particle size was determined from a minimum of 200 particles using TEM micrographs and ImageJ software developed by the National Institutes of Health. Energy dispersive spectroscopy (EDS) was used to determine the relative metal percent composition of the bimetallic species.

Catalyzed Reduction of *p*-nitrophenol

Homogeneous Catalysis

The catalytic activity of each nanoparticle species was assessed by a model chemical reaction in which *para*-nitrophenol is reduced to *para*-aminophenol with the addition of BH_4^-. A solution of 6.0 mM *p*-nitrophenol was prepared at pH 10 using 0.1M NaOH. A red shift from 317 to 400 nm is observed with the increased pH of the alkaline solution due to the formation of the nitrophenolate ion.[1] UV-Vis spectroscopy was used to monitor the absorbance at 400 nm, which remains unchanged in the absence of catalyst. Calculated volumes of 0.04 mM DEN solution and 6.0 mM of *p*-nitrophenol were added to a 1.0 cm quartz cuvette. 0.1 M of BH_4^- was then added to the cuvette while stirring. The spectrophotometer was configured to simultaneously begin recording absorption spectra with a cycle time of 0.5 s. The absorbance at 400 nm decreased and a new peak assigned to *p*-aminophenol emerged at 310 nm. As the

reaction progressed, the pale yellow color of *p*-nitrophenol disappeared, corresponding to the loss of absorbance from the visible spectrum. Endo et al.[10] has reported the reduction of *p*-nitrophenol as a pseudo-first-order reaction when sodium borohydride was present in large excess. A rate constant, *k*, can be extracted by monitoring the absorbance at 400 nm and fitting this data to the equation $\ln A_{400} = -kt + \ln A_{400,\, t=0}$ where A_{400} is the absorbance at 400 nm and $A_{400,\, t=0}$ is the absorbance at 400 nm at time 0 s.

Heterogeneous Catalysis

A three-electrode setup was used for all electrochemical experiments, where a gold wire functioned as the counter and all potentials were measured against a Hg/Hg_2SO_4 reference electrode. Glassy carbon electrodes were initially electrooxidized in 0.5M H_2SO_4 by holding the potential at 1.2V versus Hg/Hg_2SO_4 to create phthalic anhydride functionalities on the GCE surface[12]. The phthalic anhydride groups are speculated to undergo nucleophilic attack by the peripheral hydroxyl groups of the dendrimer, robustly attaching the DENs to the glassy carbon surface through ether linkages.[13] The heterogeneous catalytic activity was assessed using cyclic voltammetry and a 3-electrode setup, where the G6-OH DEN/GCE functioned as the working electrode. A measure of the potential at which PNP was reduced to PAP gives a relative idea of the catalytic activity of the dendrimer-encapsulated nanoparticles. A rate constant (*k*) can be determined by measuring the cathodic current density (*j*) for several concentrations of *p*-nitrophenol and then plotting the log of the current density versus the log of PNP concentration, as given by the equation $\log(j) = n \log[PNP] + \log(k)$.[14]

Results and Discussion

Particle size distributions for both G4-NH_2 and G6-OH DEN samples were determined using high resolution transmission electron microscopy (HRTEM). As seen in images of the DENs and corresponding histograms in Figures 4 and 5, a high degree of monodispersity was achieved in all samples.

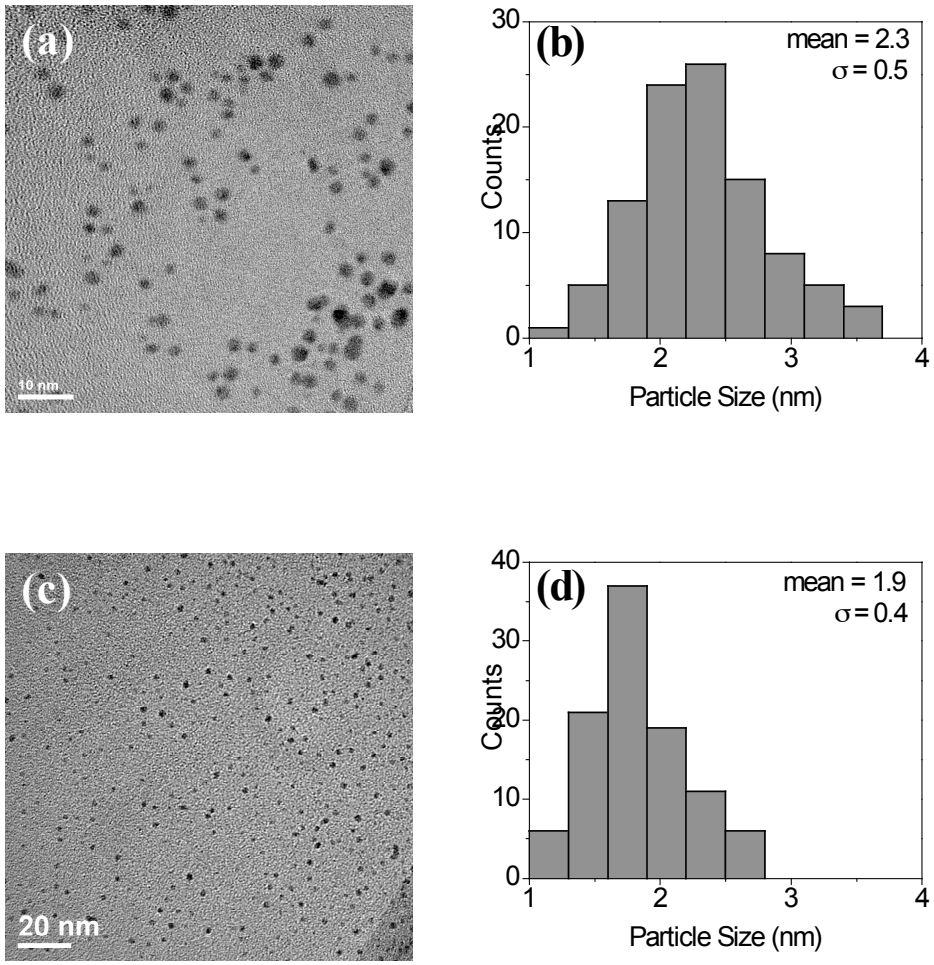

Figure 4 Representative TEM images for G4-NH_2 dendrimer-templated nanoparticles (a) Au and (c) Pt. Corresponding particle size histograms (b) Au and (d) Pt.

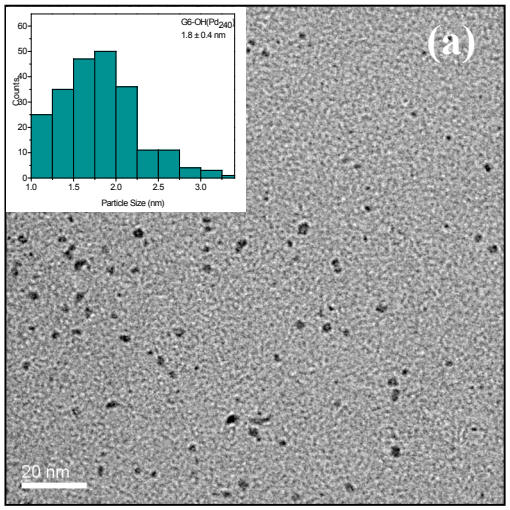

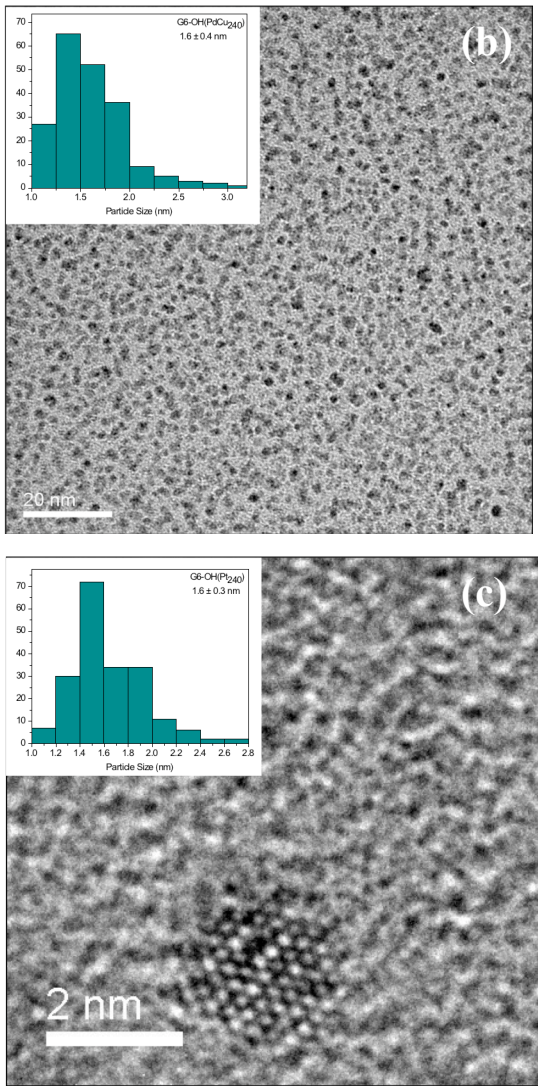

Figure 5 Representative TEM images of G6-OH dendrimer-encapsulated nanoparticles (a) Pd (b) PdCu (c) Pt

Lattice structures visible on the nanoparticle surfaces at higher magnification suggest that the DENs are crystalline structures. Particle sizes were determined from an average of 100-200 randomly selected particles in the TEM images using ImageJ software. The average particle sizes for Au, Pd, Pt, AuCu, PdCu, and PtCu were all found to be less than 2.5 nanometers in diameter, which is consistent with nanoparticles encapsulated within 4.5 nm G4-NH_2 or 6.7 nm G6-OH dendrimer templates.[6] Copper DENs are speculated to appear larger in TEM micrographs because of metal oxide layers that form on the surface of the particles. A solution of G4-NH_2 Cu

DENs exposed to air was oxidized to a blue Cu^{2+} solution within an hour. Cu DEN solutions purged with Ar remained stable for a longer time but eventually oxidized to Cu^{2+}.

Bimetallic DENs were synthesized in order to investigate the possibility of achieving a greater rate of catalysis by creating lattice structures with synergistic properties. The synergistic effects of combining two metals have been reported for many other reactions as well as for the reduction of *p*-nitrophenol using AuAg nanoparticles.[10] The average diameter for G6-OH PtCu bimetallic DENs was found to be 1.8 ± 0.3 nm, 1.6 ± 0.4 nm for PdCu, and 2.0 ± 0.6 nm for AuCu. As shown in Figure 6, energy dispersive spectroscopy (EDS) was used to determine the relative atomic percentages of metals within the bimetallic particles. Differences between the theoretical (1:1) and experimental ratios for bimetallic particles are attributed to the differing affinities of the metal ions for the interior tertiary amines.

Sample	Particle Size (nm)	Atomic %
G6-OH(Au_{240})	1.7 ± 0.4 nm	100% Au
G6-OH(Pd_{240})	1.8 ± 0.4 nm	100% Pd
G6-OH(Pt_{240})	1.6 ± 0.3 nm	100% Pt
G6-OH(Cu_{240})	2.3 ± 0.4 nm	100% Cu
G6-OH($AuCu_{240}$)	2.0 ± 0.6 nm	79.3% Cu / 20.7% Au
G6-OH($PdCu_{240}$)	1.6 ± 0.4 nm	45.6% Cu / 54.4% Pd
G6-OH($PtCu_{240}$)	1.8 ± 0.3 nm	86.3% Cu / 13.7% Pt

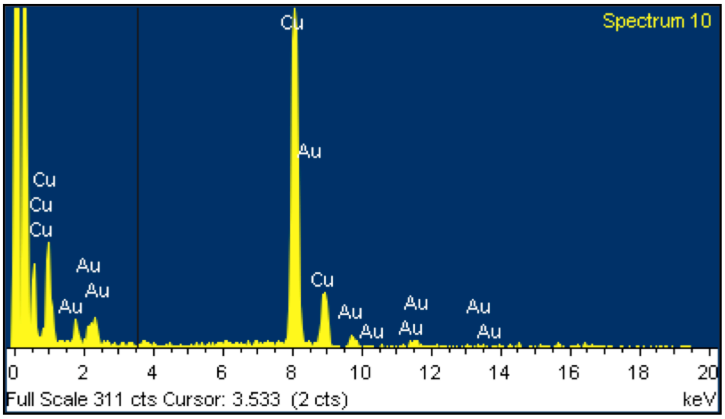

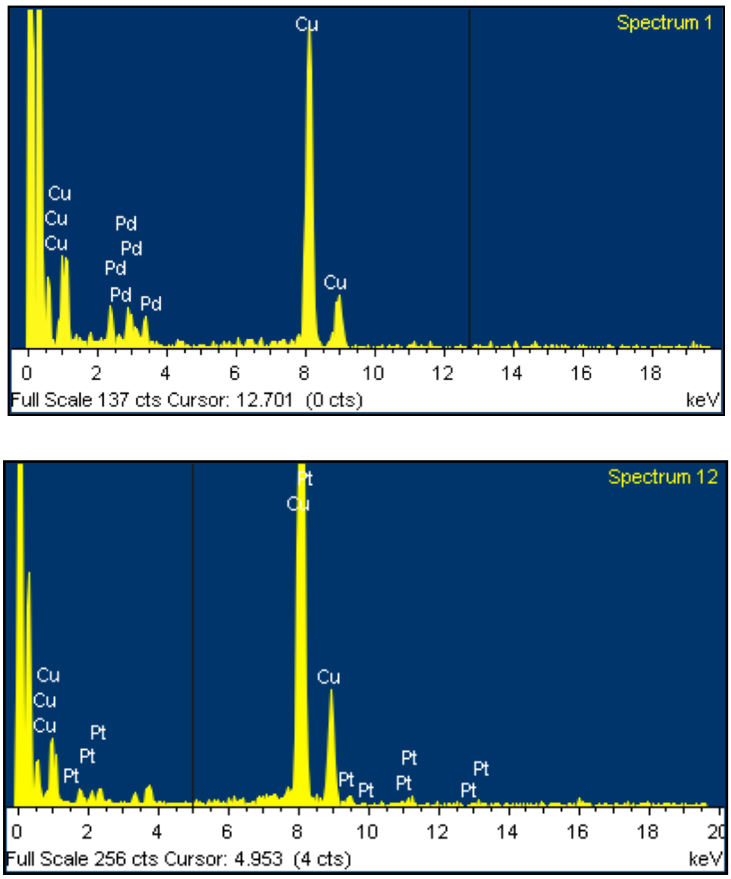

Figure 6 Table of G6-OH DEN particle sizes and relative atomic percentages determined using energy dispersive spectroscopy. Single-particle EDS spectra are representative of all bimetallic samples.

The catalytic activity of each system was assessed based on the rate of reduction of *p*-nitrophenol to *p*-aminophenol. Homogeneous catalytic activity was determined by monitoring the absorbance of the nitrophenolate ion at 400 nm in alkaline conditions. As the reaction proceeded, the absorbance for *p*-nitrophenol disappeared and a new peak attributed to *p*-aminophenol emerges at 310 nm (Figure 7).

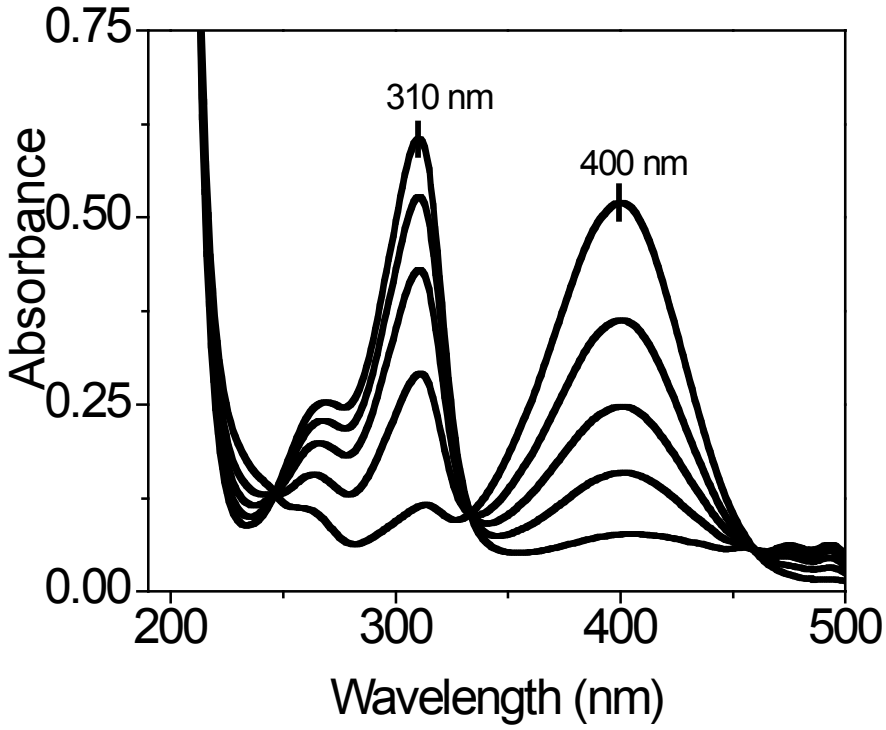

Figure 7 UV-Vis spectra for the reduction of *p*-nitrophenol (400 nm) at 1.9 ± 0.4 nm G4-NH_2 Pd-DENs. The reaction was monitored for 200 seconds with a cycle time of 0.5 s. Spectra were edited for clarity.

This corresponds visually with the disappearance of the bright yellow solution to form a colorless solution that absorbs in the ultraviolet region. The reaction parameters were optimized so that the absorbance of *p*-nitrophenol at λ = 400 nm was less than 1 AU and the reduction proceeded in a reasonable amount of time. Nanoparticle solutions of 0.4 uM, 1.0 uM, and 10.0 uM were analyzed and rate constants extracted to ensure that the reaction was pseudo-first order within this concentration range.

Oxidation of the nanoparticles upon exposure to air resulted in an induction period that was observed for each of the DEN samples. Metal oxides form a layer on the surface of the nanoparticle inhibiting the phenolate from binding to the surface atoms. This oxide layer was speculated to be the reason why the average G4-NH_2 Cu^0 particle was larger than calculated values. Induction periods have also been reported by Pradhan et al.[2], specifically for silver nanoparticles. However, these induction periods can be eliminated completely by first adding

sodium borohydride to the nanoparticle solution in the cuvette, followed by the addition of *p*-nitrophenol. This is consistent with the idea that the surface oxides must first be reduced by BH_4^- before the reactant can chemisorb onto the nanoparticle surface. Two different test procedures involving different addition sequences were compared and found to produce identical values for the rate constants.

The rate constants for reduction of *p*-nitrophenol shown in Figure 8 were determined by monitoring the absorbance of *p*-nitrophenol at 400 nm. A comparison of the relative rates indicates that gold was the most active monometallic catalyst for this reaction (k = 0.56 s^{-1}) whereas copper was the least active (k = 0.01 s^{-1}).

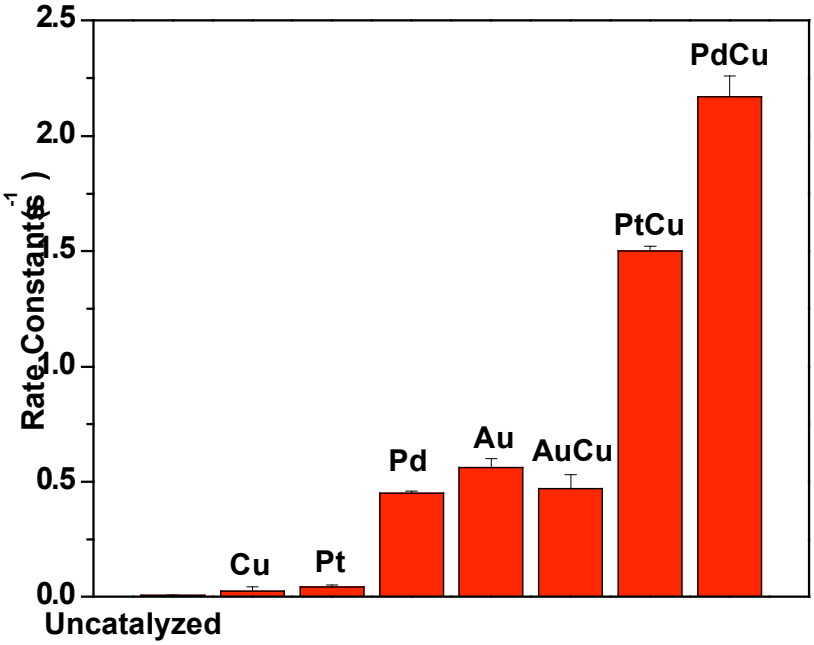

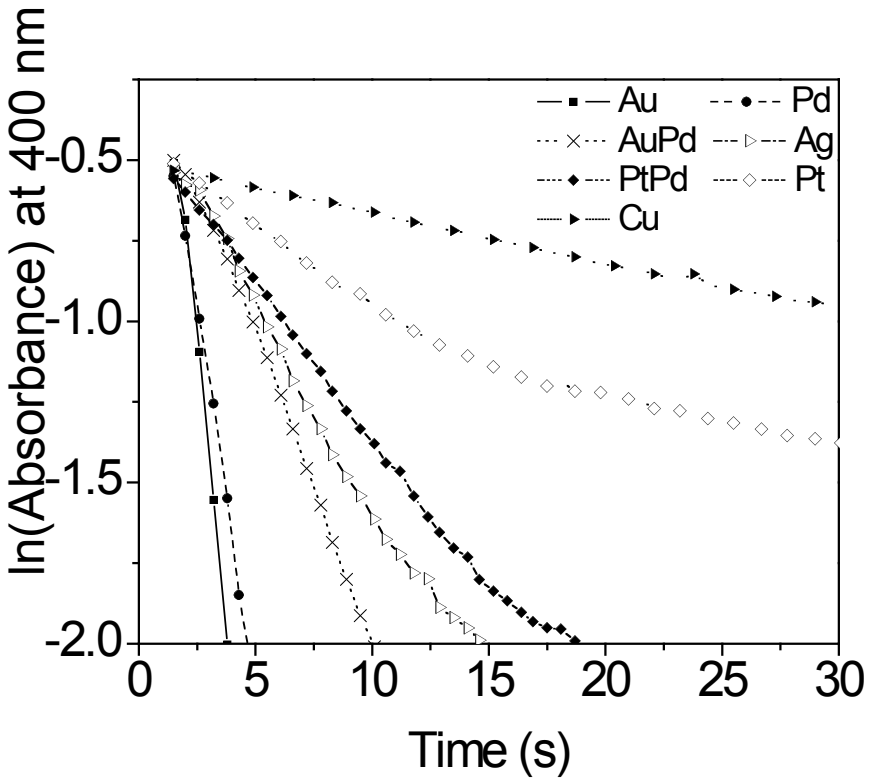

Figure 8 Plot of ln(Absorbance) versus time for the reduction of *p*-nitrophenol for all G4-NH_2 DENs.

The inactivity of copper may largely be a result of the ease with which it is oxidized. Results from this experiment also support well established concepts about the size dependent catalytic properties of metals. Various reasons can be speculated on as to why gold exhibited the greatest rate of reduction. Gold might have the highest catalytic activity because of its high electronegativity value. This higher electronegativity increases the diffusion rate of the reactants to the surface of the particle. Using electronegativity as a trend, the order of the metals would be: Au (2.4) > Pd (2.2) > Pt (2.2) > Cu (1.9). This models the order of the monometallic particles very well with the exception of Pt. The electronegativity values for Pd and Pt are identical, but their rate constants were significantly different which suggests that more than one factor contributes to catalytic activity. Other studies have shown that hydroxyl functionalities strongly adsorb onto the surface of Pt and reduce the number of active sites available for reactions like

oxygen reduction.[16] It is plausible that the Pt-DEN surface was passivated by *p*-nitrophenol reduction which would have greatly reduced its catalytic activity.

The heterogeneous catalytic activity of the nanoparticles supported on glassy carbon electrodes was assessed using cyclic voltammetry. Figure 9 shows representative cyclic voltammagrams of the G6-OH dendrimer-encapsulated particles. Upon the initial sweep from 0.2V to -1.2V, the peak located at -0.35V is absent and there is a cathodic peak located at -1.2V which corresponds to the 6 electron, 6 proton reduction of *para*-nitrophenol to *para*-aminophenol. On the reverse scan, there is an anodic current that corresponds to the oxidation of *p*-aminophenol back to the *p*-quinoneimine. On the second and subsequent scans, the cathodic peak at -0.35V grows in as a result of the rereduction of the *p*-quinoneimine back to *p*-aminophenol.

A thermodynamic argument can be made based on the reduction potential of PNP versus Hg/Hg_2SO_4, where the more catalytically active species reduce *p*-nitrophenol at more positive potentials. Based on this criteria, PdCu (E_p= -0.96V) would be the most catalytically active heterogeneous catalyst followed by AuCu (E_p= -1.03V). Rate constants can be extracted by plotting the log of the current density (*j*) versus the log of varying concentrations of PNP as shown in Figure 10. As highlighted in the table, the rate constants and reaction orders were nearly identical for all nanoparticle species.

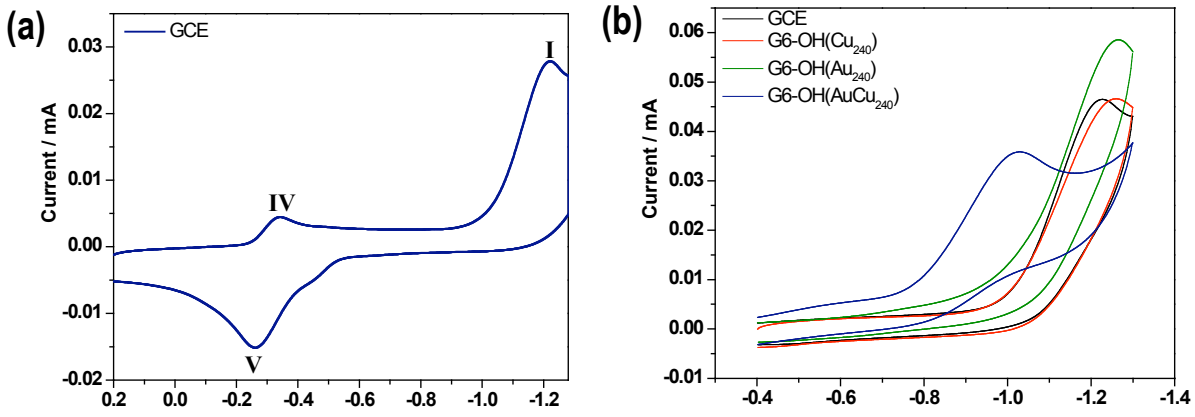

Figure 9 (a) Cyclic voltammogram of glassy carbon electrode in 3mM *p*-nitrophenol + 5mM KNO_3 (versus Hg/Hg_2SO_4) (b) Cyclic voltammograms (scan rate = 50 mVs^{-1}) of G6-OH Cu, Au, and AuCu in 5mM *p*-nitrophenol + 5mM KNO_3

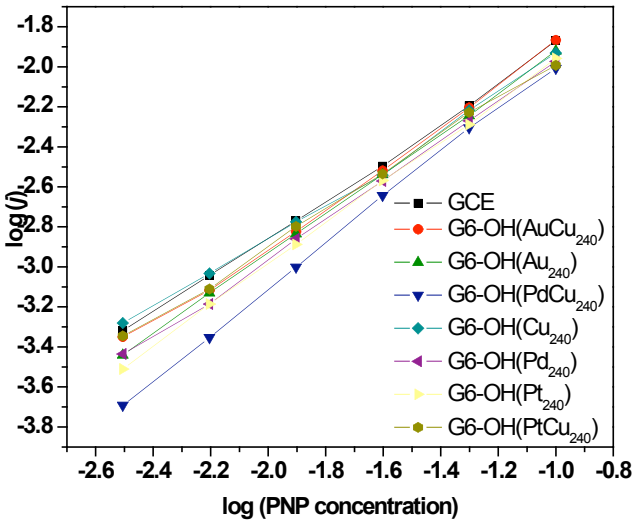

Sample	$\log j_{Ep} = \log k + n \log [PNP]$	n	k (s^{-1})
Glassy Carbon	y = 0.9552x - 0.9514	0.96	0.11
G6-OH(Au_{240})	y = 1.002x - 0.9289	1.00	0.12
G6-OH(Cu_{240})	y = 0.8947x - 1.0621	0.89	0.09
G6-OH(Pd_{240})	y = 0.9819x - 0.9954	0.98	0.10
G6-OH(Pt_{240})	y = 1.0227x - 0.9413	1.02	0.11
G6-OH($AuCu_{240}$)	y = 0.9927x - 0.9072	0.99	0.12
G6-OH($PdCu_{240}$)	y = 1.1298x - 0.8555	1.13	0.13
G6-OH($PtCu_{240}$)	y = 0.9178x - 1.0602	0.92	0.09

Figure 10 Plot of log(j) versus log[PNP] with table of rate constants (k) and reaction orders (n)

A significant increase in homogeneous and heterogeneous catalytic activity was observed for the bimetallic DENs. Microscopy analysis does not reveal whether the bimetallic particles have a core-shell or alloy structure and therefore it is difficult to determine the structural properties on the surface of these DENs. It is also not clear if the lattice structures formed with PdCu, PtCu, and AuCu are more resistant to oxide formation and favor enhanced chemisorption and turnover of *p*-nitrophenol. X-ray photoelectron spectroscopy (XPS) studies can be used to further elucidate surface properties such as the extent of oxidation. This technique coupled with EDS can be used to determine whether the bimetallic particles are alloy or core-shell structures.

Conclusion

Mono- and bimetallic particles were synthesized using G6-OH and G4-NH_2 dendrimer templates. Characterization by TEM revealed that the particles were monodisperse and of sizes consistent with dendrimer encapsulated nanoparticles. EDS was used to confirm the bimetallic

nature of the DENs and determine the metal composition of the PtCu, PdCu, and AuCu species. The catalytic activities of Au, Cu, Pd, and Pt metals were compared for their rate of reduction of *p*-nitrophenol. It was shown that gold was the most active monometallic catalyst for this reaction, and PdCu was the most active bimetallic catalyst. This study has also elucidated a synergistic catalytic effect when Cu is alloyed with a more noble metal for the reduction of *p*-nitrophenol.

Acknowledgments

Financial support for this work was provided in part by the Arnold and Mabel Beckman Foundation, the National Science Foundation and the Howard Hughes Medical Institute. I would also like to acknowledge the support of the Texas Materials Institute and the Center for Nano and Molecular Science.

References

(1) Hayakawa, K.; Yoshimura, T.; Esumi, K. *Langmuir*. **2003,** *19*, 5517-5521.

(2) Pradhan, N.; Pal, A.; Pal, T. *Langmuir.* **2001,** *17*, 1800-1802.

(3) Sanchez et al. *J. Phys. Chem. A* **1999,** *103*, 9573-9578.

(4) Manna, A.; Imae, T.; Aoi, K.; Okada, M.; Yogo, T. *Chem. Mater.* **2001,** *13*, 1674-1681.

(5) Panigrahi et al. *J. Phys. Chem. C*. **2007**, *111*, 4596-4605.

(6) Scott, R. W. J.; Wilson, O. M.; Crooks, R. M. *J. Phys. Chem. B* **2005,** *109*, 692-704.

(7) Boyen, H. –G. et al. *Science.* **2002,** *297*, 1533-1536.

(8) Zhao, M.; Sun, L.; Crooks, R. M. *J. Am. Chem. Soc.* **1998,** *120*, 4877-4878.

(9) Scott, R. W. J.; Ye, H.; Henriquez, R. R.; Crooks, R. M. *Chem. Mater.* **2003**, *15*, 3873-3878.

(10) Endo, T.; Yoshimura, T.; Esumi, K. *Journal of Colloid and Interface Science*. **2005,** *286*, 602-609.

(11) Corma, A.; Concepcion, P.; Serna, P. *Angew. Chem. Int. Ed.* **2007**, *46*, 1-5.

(12) Bustos, E. B.; Jimenez, M. G. G.; Diaz-Sanchez, B. R.; Juaristi, E.; Chapman, T. W.; Godinez, L. A. *Talanta*. **2007**, *72*, 1586-1592.

(13) Ye, H.; Crooks, R. M. *J. Am. Chem. Soc.* **2005**, *127*, 4930-4934.

(14) Ghodbane, O.; Sarrazin, M.; Roue, L.; Belanger, D. *Journal of The Electrochemical Society.* **2008**, *155*, (6), F117-F123.

(15) Esumi, K.; Isono, R.; Yoshimura, T. *Langmuir*. **2004**, *20*, 237-243.

(16) Stamenkovic, V. R. et al. *Science.* **2007**, *315*, 493-497.